Complex genotype-phenotype relationships shape the response to treatment of Down Syndrome Childhood Acute Lymphoblastic Leukaemia

Christoph Lutz[1,7,8*], Virginia A. Turati[1*], Ruth Clifford[9], Petter S. Woll[2,10], Thomas Stiehl[4], Anders Castor[5], Sally A. Clark[2,3], Helen Ferry[2], Veronica Buckle[2], Andreas Trumpp[6], Anthony Ho[7], Anna Marciniak-Czochra[4], Javier Herrero[1], Anna Schuh[9], Sten Eirik W. Jacobsen[2,10] and Tariq Enver[1]

[1]University College London, Cancer Institute, London WC1E 6BT, UK
[2]MRC Molecular Haematology Unit, MRC Weatherall Institute of Molecular Medicine, University of Oxford, Oxford, OX3 9DS, UK
[3]MRC Molecular Haematology Unit, MRC Weatherall Institute of Molecular Medicine, Flow Cytometry Facility, University of Oxford, Oxford, OX3 9DS, UK
[4]Institute of Applied Mathematics Mathematikon, Heidelberg University, Germany
[5]Department of Paediatric Haematology/Oncology, Skane University Hospital, Sweden
[6]Deutsches Krebsforschungszentrum Heideleberg (DKFZ), Germany
[7]Department of Internal Medicine V, Heidelberg University, Germany
[8]Praxis für Onkologie, Neversstrasse 5, 56077 Koblenz, Germany
[9]Department of Haematology, Oxford Radcliffe Hospitals NHS Trust, Oxford OX3 9DU, UK
[10]Center for Hematology and Regenerative Medicine, Department of Medicine Huddinge and Department of Cell and Molecular Biology, Karolinska Institutet and Karolinska University Hospital, Stockholm, Sweden
[*] These authors contributed equally to this work

Correspondence to:

Tariq Enver PhD
UCL Cancer Institute
Stem Cell Laboratory
Paul O'Gorman Building
72 Huntley Street
London WC1E 6BT

email: t.enver@cancer.ucl.co.uk
phone: +44 (0)20 7679
Fax: +44 (0)20 7679 6914

Abstract

Extensive genetic and epigenetic variegation has been demonstrated in many malignancies. Importantly, their interplay has the potential to contribute to disease progression and treatment resistance. To shed light on the complex relationships between these different sources of intra-tumour heterogeneity, we explored their relative contributions to the evolutionary dynamics of Acute Lymphoblastic Leukaemia (ALL) in children with Down syndrome, which has particularly poor prognosis. We quantified the tumour propagating

potential of genetically distinct sub-clones using serial transplantation assays and SNP-arrays. While most leukaemias were characterized by a single dominant subclone, others were highly heterogeneous. Importantly, we provide clear and direct evidence that genotypes and phenotypes with functional relevance to leukemic progression and treatment resistance can co-segregate within the disease. Hence, individual genetic lesions can be restricted to well-defined cell immunophenotypes, corresponding to different stages of the leukemic differentiation hierarchy and varied proliferation potentials. As a result of this difference in fitness, which can be accurately quantified via competitive transplantation assays, matching diagnostic, post-treatment, and relapse leukaemias can be dominated by different genotypes, including pre-leukemic clones persisting throughout the disease progression and treatment. Intriguingly, plasticity also appears to be a temporally defined property that can segregate with genotype. These results suggest that Down Syndrome ALL should be viewed as a complex matrix of cells exhibiting genetic and epigenetic heterogeneity that foster extensive clonal evolution and competition. Therapeutic intervention reshapes this 'ecosystem' and may provide the right conditions for the preferential expansion of selected compartments and subsequent relapse.

Introduction:

The existence of intra-tumour heterogeneity, both genetic and epigenetic, has been documented in both solid and haematological malignancies[1–3]. In studies of childhood acute lymphoblastic leukaemia (ALL), we and others previously used multicolour-FISH and whole genome sequencing to show that these tumours are clonally variegated, and to demonstrate through serial transplantation assays, that leukaemia tumour propagating cells (TPCs) are also genetically heterogeneous[4,5]. This finding was supported by our later genetic analysis of immunophenotypically distinct ALL diagnostic subpopulations which demonstrated similar distribution of subclones within a disease-specific primitive B-cell compartment (stemB, $34^{+}38^{-}19^{+}$) and the disease bulk in most but, crucially, not all leukaemias[6]. Such experiments

relied on high-depth bulk whole-genome sequencing followed by single-cell qPCR and, together with our earlier work, suggested that genotype and phenotypes related to differentiation stage and cell-cycle state might not necessarily co-segregate within the disease. Importantly, as chemotherapy-induced selection acts on these same phenotypic traits[6–8], this lack of segregation also underpinned the survival of most genotypes following the early stages of childhood ALL treatment (namely, induction chemotherapy – where maximum cytotoxicity is achieved); as we demonstrated using a xenograft model of transplantation and treatment of primary leukaemias[6].

Large-scale comparisons of matching diagnostic and relapse samples from paediatric ALL patients, have nonetheless previously reported that in some patients a subset of diagnostic subclones, or of their later evolutionary descendants, can be selectively enriched at the time of disease recurrence[9,10]. Assuming that these clones did not become dominant as a result of stochastic selection, this finding opens up the possibility that fitness-based genotypic selection might potentially occur on a longer timescale than that of induction chemotherapy. It is not unreasonable to speculate that in a treatment protocol that lasts up to four years even subtle differences in fitness might eventually lead to clonal dominance. Another Another possibility is that in certain settings, genotype and treatment-associated phenotypes do in fact co-segregate (either already at diagnosis or later because of further genomic evolution). In support of this latter hypothesis, our analysis of $34^{+}38^{-}19^{+}$ (StemB) BCP-ALL cells indicated that in a small proportion of leukaemias (1 out of 5 analysed), specific genotypes might indeed be preferentially enriched within developmentally more primitive and quiescent disease compartments[6]. Furthermore, recent evidence suggests that mutations induced by chemotherapy treatment itself (particularly those targeting p53) might be responsible for evolution of new and fitter subclones, inducing drug-resistance and leading to relapse[11].

To shed light on the complex genotype-phenotype relationship that shape ALL, we here conduct a comprehensive investigation into the relative contribution of different sources of intratumor heterogeneity, namely genetic makeup and epigenetically determined properties - particularly cell cycle state, TPC activity and differentiation stage - to disease initiation, progression, and treatment resistance. In doing so we focused our attention on Down's syndrome associated ALL as this rarer disease subtype has so far remained poorly characterised while being associated with considerably worse prognosis than ALL in children without Down syndrome[12,13].

Altogether our results support the idea that ALL should be viewed as a complex matrix of cells exhibiting genetic and epigenetic heterogeneity. Our work provides evidence for, in some patients, diversification in functional properties amongst immunophenotypically-distinct leukemic subpopulations. In theis setting, those rare leukemic cells which remain after induction chemotherapy, and primarily account for minimal residual disease (MRD), are highly enriched for the stemB phenotype; suggesting that the more primitive and less proliferative leukemic compartments likely constitute the pool of cells from which relapse arises. Crucially, in this setting where genotype and resistance-associated phenotypes co-segregate, bottleneck selection at phenotype level is accompanied by evidence of a clonal sweep.

Methods:

Patient samples

Diagnostic and follow-up ALL bone marrow (BM) samples were obtained after informed consent and the approval of the relevant research ethics committee from patients at the Paediatrics Haematology Unit, Lund University Hospital, Sweden. Samples from 4 children with Down's ALL were analyzed. For further patient characteristics see Table 1.

125 **Cell separation, flow cytometric analysis and cell sorting**

126 Total mononuclear cells (MNCs) were isolated from BM samples by ficoll gradient
127 centrifugation and directly cryopreserved in DMSO for later use. In some cases, $CD34^+$ cells
128 were enriched by magnetic bead separation (StemCell Technologies or Miltenyi). CD34-
129 enriched cells or MNCs were stained with anti-human CD19 PE (BD-Pharmingen), CD34
130 FITC (BD-Pharmingen) and CD38 APC (BD-Pharmingen). Cells were resuspended in
131 staining buffer containing 10%FBS, DAPI at 0·1μg/ml and flow cytometric analysis and cell
132 sorting was perfomed using a BD FACSAriaII cell sorter using FACSDiva Software v6.0 (BD
133 Biosciences). Cell subsets were defined as I.) HSC ($34^+38^-19^-$) II.) Stem/B ($34^+38^-19^+$) III.)
134 Progenitor ($34^+38^+19^-$) IV.) ProB ($34^+38^+19^+$) and V.) PreB/Mature B-cells (34^-19^+). Further
135 data analysis was performed using FlowJo v10.7 (Tree star) software.

136

137 **Cell cycle analysis of leukaemia subpopulations**

138 Cells were stained with anti-himan CD19-PECy5 (BioLegend), then fixed and permeabilized
139 with 1.6% paraformaldehyde and 90% ice-cold methanol. This was followed by staining with
140 anti-human CD34-APC (BD), CD38-PETxR (Invitrogen) and Ki67-FITC (Becton-Dickinson).
141 For DNA content analysis cells were incubated with 0·5μg/mL DAPI. Stained cells were
142 analyzed on a FACS LSRII SORP using FACSDiva Software v6.0 (BD Biosciences).

143

144 **FISH analysis**

145 Cells were fixed on slides in methanol/acetic acid fixative (3:1 vol/vol) and then hybridized
146 with BCR-ABL1 FISH probes using the LSI BCR/ABL1 Dual Color Dual Fusion Translocation
147 probes (Abbot). The slides were analyzed with an Olympus BX51 microscope equipped with
148 epifluorescence and a triple band pass filter. Images were captured by using a Sensys
149 charge-coupled device camera (Photometrics, Tucson, AZ) and MacProbe software (Applied
150 Imaging, Newcastle upon Tyne, U.K.). When possible, and unless otherwise specified at
151 least 100-150 nuclei were analyzed in each sample.

152

153 **SNP-Array**

154 SNP-Arrays we performed as previously describe in Schuh et al., 2012[14].

155

156 **NSG-mouse transplantation assay**

157 Primary childhood BCP-ALL cells were transplanted into 8-12 weeks old NOD/SCID IL2Rγ^{null}
158 (NSG) sub-lethally irradiated mice (either females or males) via intramedullary injection. To
159 minimize possible adverse effects of sublethal irradiation, mice were administered acid water
160 for a week prior to the procedure, and Baytril (resuspended at 25.5 mg/kg in the drinking
161 water) for the 2 weeks following it. Sub-lethal irradiation was achieved with a single dose of
162 375 cGy. Unless otherwise stated, each mouse received 2 x 10^5 primary leukaemia cells
163 resuspended in 40µl PBS 0.5% FBS. In the case of secondary limiting dilution assays, a
164 specified equal dose of treated and control leukemic cells harvested from the BM of primary
165 recipients was injected. Twelve-week post-injection mice were sampled by BM aspiration
166 and the percentage of human engraftment was evaluated by flow cytometry
167 (hCD45/(hCD45$^+$ + mCD45$^+$)). At the same time, human cells were also FACS sorted for
168 downstream applications. Mice displaying at least 70% human engraftment were then
169 randomly assigned to either control or treatment groups (see below for details on the
170 treatment protocol). At the end of the treatment window all mice were culled, and their tibias,
171 femurs, pelvises, spleen, and brain harvested, and cells were then stained for flow cytometry
172 analysis (see above).

173

174 **Modeling of clonal evolution**

175 To reconstruct the clonal composition of the samples, we developed an algorithm similar to
176 Stiehl at al., 2021[15], which is tailored to the specific data generated in this study. The
177 algorithm systematically generates all possible combinations of different clones and checks
178 for each combination whether it can explain the experimental data. This is done by
179 expressing the allele frequencies in the data as a linear combination of the clones present in
180 the sample. Whenever there exists a linear combination with positive coefficients summing
181 up to 100%, the considered combination of clones is in line with the data. Details are
182 provided in the supplementary materials.

183

184 **Small cell numbers RNA sequencing**

185 Equivalent cell numbers (400 cells per sample) were flow sorted directly into 800µl Trizol
186 reagent (Invitrogen) and snap frozen in dry ice (long term storage at -80C). At the time of
187 extraction, the samples were thawed at RT and 160ul of chloroform was added to each.
188 Following a centrifugation step the RNA was isolated from the aqueous phase and
189 precipitated through the addition of equal volumes of isopropanol supplemented with 20µg
190 linear polyacrylamide. Samples were washed twice in 80% ethanol (first wash over night at
191 4°C, second wash 5 minutes at RT). RNA pellets were resuspended in 3-15µl of
192 diethylpyrocarbonate treated water (DEPC). RNA was then quantified by loading of 0.5-1ul
193 on an Agilent Bionalyser RNA 6,000 pico chip. Where possible equivalent amounts of total
194 RNA (100pg) from all samples were used for first strand synthesis with the SmartERv3 kit
195 (Takara Clontech) followed by 15-18 cycles of amplification (according to manufacturers'
196 instruction). cDNA was purified on Agencourt AMPureXP magnetic beads, washed twice
197 with fresh 80% ethanol and eluted in 17µl elution buffer. 1µl cDNA was quantified with Qubit
198 dsDNA HS (Molecular Probes) and checked on an Agilent Bioanalyser high sensitivity DNA
199 chip. Sequencing libraries were produced from 150pg input cDNA using Illumina Nextera XT
200 library preparation kit. A 1:4 miniaturized version of the protocol was adopted (see "Fluidigm
201 Single-Cell cDNA Libraries for mRNA sequencing", PN_100-7168_L1). Tagmentation time
202 was 5mins, followed by 12 cycles of amplification using Illumina XT 24 or 96 index primer kit.
203 Libraries were then pooled (1-2ul per sample depending on the total number of samples)
204 and purified with equal volumes (1:1) of Agencourt AMPureXP magnetic beads. Final elution
205 was in 66-144ul of resuspension buffer (depending on the total number of pooled samples).
206 Libraries were checked on an Agilent Bioanalyser high sensitivity DNA chip (size range 150-
207 2000bp) and quantified by Qubit dsDNA HS (Molecular Probes). Libraries were sequenced
208 on Illumina® NextSeq 500 using 150bp paired end kits as per manufacturer's instructions.

209

Bioinformatics

Bulk RNAseq data were processed with the nf-core/rnaseq pipeline (v1.1-blic; https://github.com/UCL-BLIC/rnaseq). Reads were initially trimmed with TrimGalore! v0.5.0 (https://github.com/FelixKrueger/TrimGalore) and aligned with STAR v2.7.0d[16]. Gene expression was quantified with featureCount v1.6.3[17]. Quality was assessed with FastQC v0.11.8 (http://www.bioinformatics.babraham.ac.uk/projects/fastqc/) and RSeQC v2.6.4[18] and summarised with MultiQC v1.6[19]. The gene expression matrix was analysed with DESeq2 v1.26.0[20] for data transformation, outlier detection, normalization, PCA and differential gene expression analyses. All analyses use vst (variance stabilizing transformation) transformed data. A PCA analysis with the top 500 most variable genes highlighted an outlying sample that was removed from downstream analysis. Gene expression signatures for B-cell lineages[21], BCR signaling, and B-cell differentiation[22] were mapped on the PCA by calculating the arithmetic mean of the PC contributions from the gene in the signatures. Gene Set Enrichment Analysis (GSEA) was performed with the fgsea v1.12.0 R package[23] using the following signatures: Hallmark from MSigDB[24], B-cell lineage[21], cell-cycle state[25] and BCR signalling[22].

Data availability

SNP-array and RNAseq data are available at EGA under accession number EGAS00001005968.

Results

We here explored the role of intra-tumour heterogeneity in the progression and response to treatment of Down's Syndrome-associated ALL. We initially focused on genetic variegation and described the phylogenetic hierarchies of diagnostic material from 4 patients. Serial transplantation of bulk ALL samples into immune-deficient NSG-mice was concomitantly utilized to evaluate the tumour propagating potential and dynamic behaviours of the different

237 subclones identified. SNP-arrays were performed on diagnostic specimens as well as cells
238 isolated from the BM of primary and secondary transplanted mice (see schemata in Figure
239 1A). In patients 1, 3 and 4, a single dominant clone was detected both at diagnosis and in all
240 primary and secondary transplanted mice (Figure 1B). In patient 2, instead, a more complex
241 picture was observed, with several subclones coexisting within the tumour and contributing
242 to a different extent to engraftment across recipients. In this patient we detected two
243 deletions on chromosomes 9 and 14 respectively, as well as an amplification on
244 chromosome X (Figure 1C). Considering the mutational mosaicism, we identified in some of
245 the engrafted mice, these observations allowed reconstruction of a simple clonal
246 phylogenetic architecture (Figure 1D, and Supp Material for Mosaicism data). However, a
247 higher-depth genetic analysis of chromosome 9 suggested a far more complicated clonal
248 landscape. A heterozygous chromosome 9 deletion was detected across engrafted animals
249 with different degrees of homozygous involvement: to the extreme of copy neutral loss of
250 heterozygosity (cnLOH) (Figure 2A). A simple explanation to this observation is that pre-
251 existing sub-clones present at diagnosis at sub-threshold levels, were expanded through
252 secondary transplantation until reaching detection levels. Alternatively, continuous
253 broadening of the chromosome 9 deletion could have occurred over the short time frame of
254 the serial transplantation assays. This latter hypothesis would be indicative of active ongoing
255 clonal evolution. Based on the mosaicism data, and assuming no new mutations developed
256 during transplantation, we were able to reconstruct a more comprehensive phylogenetic tree.
257 To do so, we developed a custom-made computational model which we used to calculate all
258 the theoretically possible diagnostic clone-combinations supported by our SNPs data
259 analysis (Supplementary Table 1). In total 15-28 diagnostic clones were necessary to
260 explain the mutational read-out from the xenografts. Of note, since SNP-arrays are limited in
261 both genomic resolution (i.e., deletion size) and sensitivity to low abundance copy number
262 variants (CNV) it is possible that our model might underestimate the number of clones
263 (Figure 2B and supplementary methods). Nonetheless, this finding clearly illustrates the high

264 clonal complexity of ALL and is in line with our earlier single-cell WGS based
265 characterization of genetic heterogeneity in non-Down Syndrome ALL, which also identified
266 branching clonal architectures with up to 19 descendant subclones[6].
267
268 We subsequently sought to shed light on the phenotype-genotype relationship that defines
269 the properties of individual leukemic subclones, by performing SNP analysis on bulk tumour
270 cells and flow-sorted immunophenotypically-distinct ALL subpopulations from two Down's
271 syndrome ALL patients (Patient 2 and 3), both before and after xenotransplantation (Figure
272 3A and Supplementary Figure 1). In this analysis we detected identical clonal architectures
273 within diagnostic bulk, stemB and proB cells isolated from each patient leukaemia (Figure
274 3BC). All samples analysed from patient 3 confirmed the existence of a single dominant
275 leukemic clone (Figure 3C and supplementary table 1). In addition to the founding
276 chromosome 21 amplification, the third patient (Patient 4) we examined harboured a BCR-
277 ABL translocation. FISH analysis showed that in this leukaemia the fusion gene marked
278 proB- and preB-like sub-compartments, but not cells with the more primitive and disease-
279 specific stemB ($34^{+}38^{-}19^{+}$) phenotype[26] (Figure 4A). Surprisingly, in serial transplantation
280 experiments flow-sorted stemB cells only gave rise to grafts with stemB like cells but not
281 more differentiated (proB-preB) B-cell phenotypes. These stemB like grafts remained BCR-
282 ABL-negative. Similarly, proB cells derived grafts only contained proB and preB cells, all of
283 which retained the BCR-ABL-fusion. Collectively these data suggest lack of phenotypic
284 plasticity amongst diagnostic cells from this patient.
285
286 We next compared the relative fitness of the two subpopulations (stemB and proB) in a
287 competitive transplantation setting facilitated by (i) the presence of the BCR-ABL
288 translocation as a clonotypic marker and (ii) the non-interchangeability of their
289 immunophenotypes. We transplanted NSG-mice with different ratios of stemB and proB ALL
290 cells and read out engraftment. In all cases the BCR-ABL^{+} proB cells displayed increased

291 engraftment fitness, most clearly exemplified in the setting where proB cells represented
292 only 10% of the initial inoculum and yet constituted 95% of the resultant leukaemia (Figure
293 4B). Reasoning that enhanced fitness may stem from a proliferative advantage we next
294 analysed the cell cycle status of engrafted cells. In all engrafted recipients proB cells
295 displayed a more active cycling status compared to their stemB counterparts, which had a
296 significantly larger proportion of dormant (G_0) cells (Figure 4C and Supplementary Figure 2).
297
298 We subsequently speculated that the different cycling properties of these compartments
299 could be expected to affect their relative sensitivity to therapy. To experimentally determine
300 how these different ALL sub-compartments behaved during therapy, we analysed leukemic
301 subpopulations from serially collected diagnosis, remission, and relapse samples. ProB-like
302 ALL cells were indeed preferentially eradicated during chemotherapy with only stemB ALL
303 cells remaining robustly detectable during remission (Figure 5A). After induction
304 chemotherapy extremely few proB-like cells remained, none of which carried the BCR-ABL
305 translocation. While the behaviour of these subpopulations during treatment contrasts starkly
306 with their fitness as assessed by xenotransplantation, it is entirely consistent with the known
307 relative vulnerability of cycling versus dormant cells to chemotherapy. Similarly, to what
308 previously observed in the context of bacteria and antibiotics resistance, these data also
309 support the idea of the existence of a trade-off on phenotypic traits between environments
310 with and without drug[27]. The reduced competitive ability of the less proliferative species
311 (stemB cells) in the absence of treatment hence becomes an advantage in the presence of
312 chemotherapy, while the highly proliferative proB cells pay a cost to their initial fitness.
313
314 Interestingly, the relapse sample was populated by both stemB and proB-like cells (Figure
315 5A). However, in contrast to the situation at diagnosis leukemic proB cells present at relapse
316 were BCR-ABL-negative (data not shown) and both relapse stemB and proB cells showed
317 phenotypic plasticity upon serial transplantation (Figure 5B). This data is somewhat

318 counterintuitive in that it argues against the simplest origins of relapse from the predominant
319 stemB or proB clones present at diagnosis. The stemB compartment at presentation lacked
320 phenotypic plasticity in that it was unable to regenerate proB- or preB-like cells. Since the
321 proB cells at relapse were BCR-ABL-negative, relapse could also not have been seeded by
322 the predominant diagnostic proB-like compartment that was positive for BCR-ABL.
323
324 Taking advantage of the xenograft system further investigated the phenotypic properties of
325 diagnostic and relapse cells at the molecular level by performing small cell number bulk RNA
326 sequencing (RNAseq) on cells harvested from either primary and or secondary xenografts.
327 We hence characterised six distinct cell populations i) diagnostic stemB cells, ii) diagnostic
328 proB cells iii) relapse stemB cells harvested from secondary xenografts injected with stemB
329 cells isolated from primary xenografts iv) relapse proB cells harvested from secondary
330 xenografts injected with stemB cells isolated from primary xenografts, v) relapse proB cells
331 harvested from secondary xenografts injected with proB cells isolated from primary
332 xenografts, and vi) relapse stemB cells harvested from secondary xenografts injected with
333 proB cells isolated from primary xenografts. Principal Component Analysis (PCA) showed
334 clustering of samples based on disease stage. Interestingly, diagnostic cells also clustered
335 separately based on differentiation state, while all relapse populations clustered closely
336 together (Figure 5C). This finding resonates well with our observation that in this patient
337 leukaemia, relapse but not diagnostic cells displayed high cell plasticity. While the PC1
338 component of the PC captured most of the sample variance (47.15), PC2 clearly separated
339 diagnostic proB cells and all relapse subpopulations from diagnostic stemB cells. Pathways
340 analysis on the genes driving this PC component revealed enrichment for TNF-alpha via NF-
341 KB signalling cascade (Supplementary Figure 3C), which has previously been implicated in
342 regulation of cell survival, proliferation and stemness[28].
343 Gene set enrichment analysis (GSEA) using publicly available gene expression
344 signatures[29,21] also validated our flow cytometry analysis results in that compared to

345 diagnostic proB cells and relapse cells, diagnostic stemB cells downregulated cell
346 proliferation associated genes and expressed higher levels of markers typical of more
347 immature stages of the haematopoietic and B-cell differentiation hierarchy (such as HSC and
348 MLP cells) (Figure 5C-D and Supplementary Figure 3A-B). Most B-lineage cells from ALL
349 patients are thought to be arrested at some point of the transition from the proB to preB
350 stage, therefore broadly allowing the classification of ALL leukaemias into two distinct
351 subtypes based on preBCR function. Those arrested at the preBI stage rely upon
352 IL7R/STAT5 signaling (preBCR$^-$), while those arrested at preBII stage signal by the preBCR
353 (preBCR$^+$)[22]. The frequency of pre-BCR$^+$ or pre-BCR$^-$ cases has also been suggested to
354 associate with different cytogenetic subtypes of childhood ALL. For example, the majority of
355 BCR-ABL1$^+$ leukaemias tend to display constitutive active cytokine signalling via activation
356 of STAT5 and repression of BCL6. Herein, however, we found that these two genetically and
357 phenotypically distinct disease subsets can coexist within the same leukaemia. Interestingly,
358 contrary to expectations, diagnostic proB cells, which carried the BCR-ABL translocation and
359 expressed markers associated with later stages of the B-cell differentiation (Figure 5C),
360 displayed stronger expression of the preBCR receptor components and signalling cascade,
361 while the BCR-ABL$^-$ diagnostic stemB cells preferentially upregulated various genes involved
362 in the STAT5 signalling pathway (Supplementary Figure 3D).
363
364 We subsequently used SNP arrays to genetically characterise different phenotypic
365 compartments at presentation, relapse and after serial transplantation and track the
366 phylogenetic origins of the relapse propagating clones (Figure 6). SNP analysis of the
367 relapse samples indicated that it lacked several of the distinctive genetic abnormalities which
368 characterised either the dominant stemB compartment at diagnosis or the dominant proB.
369 However, the relapse hierarchy shared with the diagnostic compartments deletions on both
370 chromosomes 12 and 14. Of note, diagnosis and relapse clones also shared a common VDJ
371 rearrangement (data not shown).

372

373 Altogether, this data implies the survival over treatment of a common evolutionary ancestor
374 not detectable at diagnosis which gave rise to the relapse hierarchy through further
375 diversification. Accordingly, analysis of a bulk remission sample identified mosaic deletion of
376 chromosome 14 in the absence of del12 and any other obvious genetic abnormality.
377 Therefore, suggesting that this mosaic deletion is not a germline event and, likely, the
378 earliest genomic alteration (also preceding del12). To understand the basis of the mosaicism
379 observed in the remission sample, we separated CD3+ and CD3- cells and performed SNP
380 analysis. The CD3- compartment contained no evidence of the del14. In contrast the CD3+
381 cells showed a complex pattern of chromosome 14 deletions indicative of a progressive
382 multi-step evolutionary process (Supplementary table 2). We next traced these del14
383 variants back to the diagnostic and relapse stemB and proB compartments, as well as the
384 CD3+ compartment isolated at diagnosis. This spectrum of 14 deletions provides a branched
385 framework for subsequent evolution of stemB and proB clones seen at diagnosis and
386 relapse. Thus, using chromosomal deletions as markers of lineal ancestry we have here
387 reconstructed the evolutionary history of a Down's ALL from the predisposing event (Trisomy
388 21), through the acquisition of initiating lesions giving rise to a preleukemic hierarchy, into
389 further transformation marked by the onset of frank leukaemia. We also monitored the
390 response of this complex leukemic hierarchy to chemotherapy through the analysis of
391 matching remission and relapse specimens. Beyond the genetic considerations our work
392 emphasizes the role of cellular state primarily at the level of dormancy and cell cycle
393 indicating vulnerability to chemotherapy.

394

395 **Discussion**

396 Many studies have explored the extent and impact of different, individually assessed,
397 sources of intratumor heterogeneity on the evolution of tumours (particularly under
398 treatment). Our work, however, argues that cancer should be viewed as a complex matrix of

399 genetic and epigenetic heterogeneity such as cellular phenotype and cell cycle properties
400 which, altogether rather than in isolation, provide a substrate for tumour evolution during
401 disease progression in response to the selective pressure exercised by therapeutic
402 interventions.
403
404 The idea that epigenetically determined cell states, contribute to functional heterogeneity
405 amongst tumour cells by controlling fundamental cellular properties such as, for example,
406 cell identity, phenotype and cell-cycle stage is paradigmatically exemplified by the cancer
407 stem cell (CSC) hypothesis; which postulates that cells within a tumour are organized in a
408 hierarchical fashion reflecting lineage relationships and tumorigenic potential, and that the
409 maintenance of cancer clones is uniquely dependent on the most primitive CSCs with self-
410 renewal capacity[30–32]. This notion, which was pioneered in the context of blood malignancies,
411 remains however extensively debated. While phenotypic heterogeneity - primarily at the level
412 of immune-phenotype – has been widely observed in ALL, disparate data exist concerning
413 the existence of leukaemia stem cells (LSCs) within this disease. Earlier work by Rehe et al.,
414 showed that many cellular fractions contain LSC-potential at a similar frequency and that the
415 majority of - if not all - cells may be able to propagate the disease[33]. Importantly, the same
416 study also found evidence for phenotypic plasticity within different subpopulations upon
417 serial transplantation in immune-deficient mice. Rare LSCs have nonetheless been
418 conclusively identified in acute myeloid leukaemia (AML), where functional evidence for their
419 existence has been provided[34–37]. However, even in this context, their exact phenotype
420 remains elusive, with more recent studies uncovering LSC activity across different cellular
421 subsets[38]. We here provide evidence that although different Down's ALL disease
422 compartment can all contribute to leukaemia propagation *in vivo,* these same compartments
423 display largely distinct fitness; both in the presence and in the absence of chemotherapy. In
424 this scenario, more primitive stem-like disease compartments are outcompeted by highly
425 proliferative early-B cell progenitors in the absence of treatment. However, this selective

426 advantage is reversed in the presence of chemotherapy, which selects for quiescent cells.
427 While the genetically heterogenous nature of childhood ALL has been demonstrated by
428 multiple earlier studies, our current work provides the first direct evidence for genetic
429 diversity of cancer propagating cells in patients with Down's syndrome ALL. Our SNP array
430 analysis of serially transplanted ALLs shows that leukemic cells undergo a process of
431 gradual branching clonal evolution demonstrated by the coexistence within a leukaemia of
432 multiple subclones bearing alterations of the same genomic locus characterised by distinct
433 breakpoints.
434
435 Our earlier work showed that in many ALL leukaemias genotype and phenotypes with
436 relevance to chemoresistance do not segregate. As a result, induction chemotherapy does
437 not select at the level of genotype. We here identified and studied the evolutionary history of
438 an unusual case of BCR-ABL+ Down's ALL in which genotype and phenotype do instead
439 clearly segregate. In this patient's leukaemia the stemB cells were fusion-gene-negative
440 while proB/pre-B cells were fusion-gene-positive. This case allowed us to reconstruct in
441 detail the complex genotype-phenotype relationship characterizing different leukemic cell
442 fractions labelled by both distinct genetic makeup and fitness. We hence observed that
443 highly quiescent and developmentally more primitive cells preferentially escaped treatment.
444 As these cells carried only a subset of diagnostic genetic alterations, the relapse disease
445 was genetically divergent from the diagnostic specimen. Reconstruction of the leukaemia
446 phylogenetic tree demonstrated that the dominant population at relapse originated from a
447 rare pre-leukemic clone. This was likely present at diagnosis below detection level and, in
448 line with its likely low proliferative activity, did not extensively expand upon transplantation.
449
450 We first demonstrated the existence of pre-leukemic cells in ALL in studies of mono-
451 chorionic twins of whom one was diagnosed with TEL-AML1-positive ALL[26,39]. Blood spot
452 studies from Guthrie-cards further showed that these pre-leukemic cells can precede overt

453 leukaemia by up to 12 years and are also detectable in patients that never go on to overt
454 disease[40,41]. A case report of a 7-year old boy diagnosed with BCP-ALL with a mixed
455 lympho-myeloid phenotype previously suggested that BCR-ABL+ non-Down leukaemic cells
456 could reactivate to drive disease recurrence more than two decades from initial diagnosis[42].
457 Our new data add to our understanding of this elusive population by showing that Down
458 Syndrome BCP-ALL chr21+ cells, which have not yet acquired the BCR-ABL translocation
459 labelling the more proliferative proB compartment disease, can preferentially survive
460 chemotherapy and, therefore, represent a reservoir for relapse initiation. Whether these cells
461 are quiescent principally as a function of their unique developmental origin[43] or rather of their
462 genotype[44] or a combination of both remains to be investigated and would be important to
463 understand if new therapeutic interventions targeting these cells are to be designed. This
464 notwithstanding, pre-leukemic clones, even when rare, should clearly be considered part of
465 the fully transformed leukaemia landscape and may upon selection by therapy provide an
466 additional cellular source for subsequent relapse.
467

468 **Acknowledgments**

469 We are grateful for the support of Leukaemia and Lymphoma Research (Specialist
470 Programme Grant to TE), MRC Molecular Haematology Unit core award (SEJ.;
471 MC_UU_12009/5), Blood Cancer UK (SEJ), Swedish Childhood Cancer Fund (SEJ), the
472 National Institute for Health Research Biomedical Research Centre Programme, the CBRC,
473 UCL, Haematolinne, the Leukemia and Lymphoma Society, USA (Career Development
474 Program fellowship to PSW), the Deutsche Forschungsgemeinschaft (fellowship to CL;
475 LU1474/1-1 and programme grant as part of the Sonderforschungsbereich; SFB873,
476 Teilprojekt A13), and the Lundbeck Foundation (Fellowship "Personalized prediction of blood
477 cancer progression using clinical data and mathematical modeling" to TS). The authors
478 acknowledge the use of the UCL Myriad High Performance Computing Facility
479 (Myriad@UCL), and associated support services, in the completion of this work.

480

481 **Authorship Contributions**

482 CL and VT performed experiments; RC analysed the SNP array; JH analysed the RNAseq
483 data with input from VT; AS interpreted and supervised SNP-array data analyses; TS
484 developed the computational model; CL and PSW performed the cell cycle analysis, VB
485 carried out FISH analyses; AC provided patient data and samples; SAC, HF and PSW
486 performed cell sorting. CL, VT, SEWJ and TE designed the study and interpreted data. CL,
487 VT and TE wrote the paper with critical input from other authors.

488

489 **Conflict of Interest Disclosures**

490 The authors declare no conflict of interest.

491 **References**

492 1. Rosenthal, R., Mcgranahan, N., Herrero, J. & Swanton, C. Deciphering Genetic
493 Intratumor Heterogeneity and Its Impact on Cancer Evolution. *Annu. Rev. Cancer*
494 *Biol. 2017* **1**, 223–240 (2016).
495 2. Marusyk, A., Almendro, V. & Polyak, K. Intra-tumour heterogeneity: A looking glass
496 for cancer? *Nature Reviews Cancer* vol. 12 323–334 (2012).
497 3. Landau, D. A., Carter, S. L., Getz, G. & Wu, C. J. Clonal evolution in hematological
498 malignancies and therapeutic implications. *Leukemia* vol. 28 34–43 (2014).
499 4. Anderson, K. *et al.* Genetic variegation of clonal architecture and propagating cells in
500 leukaemia. *Nature* **469**, 356–361 (2011).
501 5. Notta, F. *et al.* Evolution of human BCR-ABL1 lymphoblastic leukaemia-initiating cells.
502 *Nature* **469**, 362–7 (2011).
503 6. Turati, V. A. *et al.* Chemotherapy induces canalization of cell state in childhood B-cell
504 precursor acute lymphoblastic leukemia. *Nat. Cancer* doi:10.1038/s43018-021-00219-
505 3.
506 7. Ebinger, S. *et al.* Characterization of Rare, Dormant, and Therapy-Resistant Cells in

507 Acute Lymphoblastic Leukemia. *Cancer Cell* **30**, 849–862 (2016).
508 8. Lutz, C. *et al.* Quiescent leukaemic cells account for minimal residual disease in
509 childhood lymphoblastic leukaemia. *Leukemia* (2013) doi:10.1038/leu.2012.306.
510 9. Waanders, E. *et al.* Mutational Landscape and Patterns of Clonal Evolution in
511 Relapsed Pediatric Acute Lymphoblastic Leukemia. *Blood Cancer Discov.* **1**, 96–111
512 (2020).
513 10. Dobson, S. M. *et al.* Relapse-Fated Latent Diagnosis Subclones in Acute B Lineage
514 Leukemia Are Drug Tolerant and Possess Distinct Metabolic Programs. *Cancer*
515 *Discov.* (2020) doi:10.1158/2159-8290.cd-19-1059.
516 11. Kirschner-Schwabe, R. *et al.* Chemotherapy and mismatch repair deficiency
517 cooperate to fuel TP53 mutagenesis and ALL relapse. *Nat. Cancer*
518 doi:10.1038/s43018-021-00230-8.
519 12. Buitenkamp, T. D. *et al.* Acute lymphoblastic leukemia in children with Down
520 syndrome: A retrospective analysis from the Ponte di Legno study group. *Blood* **123**,
521 70–77 (2014).
522 13. Xavier, A. C. & Taub, J. W. Acute leukemia in children with down syndrome.
523 *Haematologica* vol. 95 1043–1045 (2010).
524 14. Schuh, A. *et al.* Monitoring chronic lymphocytic leukemia progression by whole
525 genome sequencing reveals heterogeneous clonal evolution patterns. *Blood* **120**,
526 4191–4196 (2012).
527 15. Stiehl, T. & Marciniak-Czochra, A. Computational Reconstruction of Clonal
528 Hierarchies From Bulk Sequencing Data of Acute Myeloid Leukemia Samples. *Front.*
529 *Physiol.* **12**, 1–13 (2021).
530 16. Dobin, A. *et al.* STAR: Ultrafast universal RNA-seq aligner. *Bioinformatics* **29**, 15–21
531 (2013).
532 17. Liao, Y., Smyth, G. K. & Shi, W. FeatureCounts: An efficient general purpose program
533 for assigning sequence reads to genomic features. *Bioinformatics* **30**, 923–930

534 (2014).
535 18. Wang, L., Wang, S. & Li, W. RSeQC: Quality control of RNA-seq experiments.
536 *Bioinformatics* **28**, 2184–2185 (2012).
537 19. Ewels, P., Magnusson, M., Lundin, S. & Käller, M. MultiQC: Summarize analysis
538 results for multiple tools and samples in a single report. *Bioinformatics* **32**, 3047–3048
539 (2016).
540 20. Love, M. I., Huber, W. & Anders, S. Moderated estimation of fold change and
541 dispersion for RNA-seq data with DESeq2. *Genome Biol.* **15**, 1–21 (2014).
542 21. Laurenti, E. *et al.* The transcriptional architecture of early human hematopoiesis
543 identifies multilevel control of lymphoid commitment. *Nat. Immunol.* **14**, 756–763
544 (2013).
545 22. Geng, H. *et al.* Self-Enforcing Feedback Activation between BCL6 and Pre-B Cell
546 Receptor Signaling Defines a Distinct Subtype of Acute Lymphoblastic Leukemia.
547 *Cancer Cell* **27**, 409–425 (2015).
548 23. Korotkevich, G. *et al.* Fast gene set enrichment analysis. (2016) doi:10.1101/060012.
549 24. Liberzon, A. *et al.* The Molecular Signatures Database Hallmark Gene Set Collection
550 In Brief Through extensive automated and manual curation, Liberzon et al. provide a
551 refined and concise collection of '"hallmark"' gene sets from the Molecular Signatures
552 Database for gene set enrichment analysis. Cell Systems The Molecular Signatures
553 Database Hallmark Gene Set Collection. *Cell Syst.* **1**, 417–425 (2015).
554 25. Tirosh, I. *et al.* Single-cell RNA-seq supports a developmental hierarchy in human
555 oligodendroglioma. *Nat. Publ. Gr.* **539**, (2016).
556 26. Hong, D. *et al.* Initiating and cancer-propogating cells in TEL-AML1-associated
557 childhood leukemia. *Science (80-.).* **319**, 336–339 (2008).
558 27. Zur Wiesch, P. S., Engelstädter, J. & Bonhoeffer, S. Compensation of fitness costs
559 and reversibility of antibiotic resistance mutations. *Antimicrob. Agents Chemother.* **54**,
560 2085–2095 (2010).

561 28. Vazquez-Santillan, K., Melendez-Zajgla, & J., Jimenez-Hernandez, & L., Martínez-
562 Ruiz, G. & Maldonado, & V. NF-κB signaling in cancer stem cells: a promising
563 therapeutic target? doi:10.1007/s13402-015-0236-6.
564 29. Sergushichev, A. A. An algorithm for fast preranked gene set enrichment analysis
565 using cumulative statistic calculation. *bioRxiv* 060012 (2016).
566 30. Dick, J. E. Stem cell concepts renew cancer research. *Blood* **112**, 4793–4807 (2008).
567 31. Kreso, A. & Dick, J. E. Evolution of the cancer stem cell model. *Cell Stem Cell* **14**,
568 275–291 (2014).
569 32. Ailles, L. E. & Weissman, I. L. Cancer stem cells in solid tumors. *Curr. Opin.*
570 *Biotechnol.* **18**, 460–466 (2007).
571 33. Rehe, K. *et al.* Acute B lymphoblastic leukaemia-propagating cells are present at high
572 frequency in diverse lymphoblast populations. *EMBO Mol. Med.* **5**, 38–51 (2013).
573 34. Shlush, L. I. *et al.* Tracing the origins of relapse in acute myeloid leukaemia to stem
574 cells. *Nature* **547**, 104–108 (2017).
575 35. Velten, L. *et al.* Identification of leukemic and pre-leukemic stem cells by clonal
576 tracking from single-cell transcriptomics. *Nat. Commun.* **12**, 1–13 (2021).
577 36. Lapidot, T. *et al.* A cell initiating human acute myeloid leukaemia after transplantation
578 into SCID mice. *MacKinnon, R. Yallen. G. Sci.* **362**, 31–39 (1993).
579 37. Dick, J. E. & Bonnet, D. Human Acute Myeloid Leukaemia is organised as a heirarchy
580 that originates from a primitive haematopoetic cell. *Nat. Med.* **3**, 730–737 (1997).
581 38. Taussig, D. C. *et al.* Leukemia-initiating cells from some acute myeloid leukemia
582 patients with mutated nucleophosmin reside in the CD34- fraction. *Blood* **115**, 1976–
583 1984 (2010).
584 39. Ford, A. M. *et al.* Fetal origins of the TEL-AML1 fusion gene in identical twins with
585 leukemia. *Med. Sci.* **95**, 4584–4588 (1998).
586 40. Greaves, M. F., Maia, A. T., Wiemels, J. L. & Ford, A. M. Leukemia in twins: Lessons
587 in natural history. *Blood* **102**, 2321–2333 (2003).

588 41. Gale, K. B. *et al.* Backtracking leukemia to birth: Identification of clonotypic gene
589 fusion sequences in neonatal blood spots. *Proc. Natl. Acad. Sci. U. S. A.* **94**, 13950–
590 13954 (1997).
591 42. Ford, A. M. *et al.* Protracted dormancy of pre-leukemic stem cells. *Leukemia* **29**,
592 2202–2207 (2015).
593 43. Böiers, C. *et al.* A Human IPS Model Implicates Embryonic B-Myeloid Fate Restriction
594 as Developmental Susceptibility to B Acute Lymphoblastic Leukemia-Associated
595 ETV6-RUNX1. *Dev. Cell* **44**, 362-377.e7 (2018).
596 44. Wray, J. P. et al. Cell cycle corruption in a pre-leukemic ETV6-RUNX1 model exposes
597 RUNX1 addiction as a therapeutic target in acute lymphoblastic leukemia. *bioRxiv*
598 *Prepr.* (2021).
599

600 **Figure legends**

601 **Figure 1: Study of clonal dynamics through serial transplantation assays. A.**
602 Experimental setup. BM samples before and after serial transplantation in NSG-mice were
603 analyzed by SNP-arrays. **B.** SNP array results of patient 1. Deletions on Chromosomes 1,
604 12 and a single amplification on Chromosome 17 were identified and shown to be stable
605 during serial transplantation. Relationships between transplants recipients are indicated with
606 arrows. The colour scale ranges from red (amplification) through white (neutral, diploid) to
607 blue (deletion). **C.** SNP array results of patient 2. Deletions on Chromosomes 9, 14 and a
608 single amplification on Chromosome X were identified. During serial transplantation copy
609 number abnormalities (CNA) disappeared and re-appeared suggesting the co-existence of
610 different sub-clones. Relationships between transplants recipients are indicated with arrows.
611 The colour scale ranges from red (amplification) through white (neutral, diploid) to blue
612 (deletion). **D.** Initial reconstruction of the clonal hierarchy of patient 2 leukaemia considering
613 Chromosomes 9, 14 and X. * Indicate secondary transplants from a primary transplant for
614 which SNP-array data are unavailable due to insufficient numbers of cells for analysis.

615

616 **Figure 2: Detailed analysis on chromosome 9 reveals higher clonal complexity**
617 **(Patient 2). A.** In depth analysis of CNA on chromosome 9 during serial transplantation
618 suggests a more complex clonal hierarchy with multiple deletions of different size targeting
619 the locus and occurrence of cnLOH. Each box indicates an individual mouse. **B.**
620 Phylogenetic reconstruction of leukaemia cells based on SNP-array data obtained at
621 diagnosis and during serial transplantation. Mosaicim of CNA suggested the existence of
622 sub-clones within analyzed samples. The panel represents a summary of the minimal
623 phylogenetic trees that can explain the mutational landscape identified in the engrafted
624 leukaemias. Minimal clone numbers were obtained using a computational algorithm (see
625 supplementary materials). There exist 30 possible minimal trees, each consisting of 16
626 clones. The red nodes correspond to clones that are found in all 30 minimal trees. The green
627 and orange nodes correspond to clones that are part of 24 and 6 out of 30 minimal trees
628 respectively. The edges indicate the phylogenetic relation among the clones. The width
629 indicates in how many of the 30 minimal trees the respective edge is present. A: loss of
630 chromosome 9, B: short homozygous deletion on chromosome 9, B2: intermediate
631 homozygous deletion on chromosome 9, B3: long homozygous deletion on chromosome 9,
632 C: CnLOH on chromosome 9, D, F: copy number losses on chromosome 14, E: trisomy X,
633 trisomy 21 (present in all subclones).The presented graph depicts the minimum number of
634 diagnostic clones required to explain the mutational landscape identified in the engrafted
635 leukaemias. Minimal clone numbers were calculated by computational modelling (see
636 supplementary materials).

637

638 **Figure 3: Correlation of phenotype and genotype. A.** Experimental setup. BM bulk,
639 stemB ($CD34^{+}CD38^{-/low}CD19^{+}$) and proB ($CD34^{+}CD38^{+}CD19^{+}$) cells were analyzed by SNP-
640 arrays before and (if available) after serial transplantation in NSG mice. **B.** In patient 2 bulk,
641 stemB and proB cells showed identical CNA. Deletions are shown in red and amplifications

642 in blue. **C.** In Patient 3 animals transplanted with bulk, stemB, and proB cells showed
643 identical CNA profiles: suggesting the existence of a single dominant clone. * Indicate
644 secondary transplants from a primary transplant for which SNP-array data are unavailable
645 due to insufficient numbers of cells for analysis. Secondary transplants from StemB and bulk
646 cells did not engraft. Deletions are shown in red and amplifications in blue.
647
648 **Figure 4: Phenotypically and genetically distinct sub-clones co-exist in a case of BCR-**
649 **ABL1$^+$ ALL (Patient 4). A.** FISH analysis of leukemic subpopulations at diagnosis and after
650 serial xenotransplantation using a BCR/ABL-specific probe. To confirm the leukemic status,
651 sorted cells were analysed by FISH for the appropriate clonal marker. Presence of the
652 t(9;22) translocation is indicated by detection of one green, one red and two red-green fusion
653 signals. **B.** Competitive transplants of genetically and phenotypically distinct BCR-ABL$^+$ proB
654 (CD34$^+$CD38$^+$CD19$^+$) and BCR-ABL$^-$ stemB (CD34$^+$CD38$^{-/low}$CD19$^+$) cells. Input and output
655 ratios of the two populations in individual mice are displayed. **C.** Cell cycle analysis of
656 leukemic StemB and proB cells from competitively transplanted NSG-mice with
657 subpopulations from a BCR-ABL1$^+$ ALL patient. Percentages of cells in G_0 (DAPI$^-$Ki67$^-$), G_1
658 (DAPI$^-$Ki67$^+$) and S/G_2/M (DAPI$^+$Ki67$^+$) are shown.
659
660 **Figure 5: Selective therapy resistance of CD34$^+$CD38$^{-/low}$CD19$^+$ StemB cells in high risk**
661 **BCR-ABL1$^+$ ALL (Patient 4). A.** Flow cytometry analysis of BCR-ABL1$^+$ ALL subpopulations
662 at diagnosis, remission, and relapse (patient 4). Percentages of CD34$^+$CD38$^{-/low}$CD19$^-$
663 (HSC), CD34$^+$CD38$^{-/low}$CD19$^+$ (stemB), CD34$^+$CD38$^+$CD19$^+$ (proB) cells and
664 CD34$^+$CD38$^+$CD19$^-$ (Progenitors) in total bone marrow (BM) mononuclear cells (MNC) are
665 shown. The black boxes show the gates used for frequency calculations. Not all collected
666 events are shown. **B.** Flow cytometry analysis of BM cells from serially transplanted NSG
667 mice injected with sorted stemB and proB cells from patient 4 relapse. **C.** PCA analysis
668 based on bulk RNA sequencing of diagnostic and relapse cells harvested from primary and

669 secondary xenografts. Six different populations of cells were analysed. i) diagnostic stemB
670 cells, ii) diagnostic proB cells iii) relapse stemB cells harvested from secondary xenografts
671 injected with stemB cells isolated from primary xenografts iv) relapse proB cells harvested
672 from secondary xenografts injected with stemB cells isolated from primary xenografts, v)
673 relapse proB cells harvested from secondary xenografts injected with proB cells isolated
674 from primary xenografts, and vi) relapse stemB cells harvested from secondary xenografts
675 injected with proB cells isolated from primary xenografts. Arrows showing the contribution of
676 different gene expression signatures (calculated as per panel D) to the sample's clusters
677 biology are displayed. **D.** Gene set enrichment analysis (GSEA) for a selection of MSigDB-
678 50 Hallmark gene-sets and published signatures associated with predefined differentiation
679 stages of the B-cell ontogeny[21]. ProB diagnostic cells are compared to the stemB diagnostic
680 cells. Significance thresholds: <0.05 after adjusting for multiple testing (using the Benjamini-
681 Hochberg method).
682
683 **Figure 6: Distinct sub-clones in the BCR-ABL1$^+$ ALL and the BCR-ABL$^-$ relapse clones**
684 **are genetically related (Patient 4). A.** SNP array results of diagnostic stemB, xenografted
685 stemB, diagnostic proB, xenografted proB, diagnostic preB, relapse stemB, relapse proB
686 and MRD-negative Remission sample are displayed. A chromosome 12 deletion was
687 present in all but the remission control sample illustrating the clonal relationship of all
688 leukemic samples. CNA of diagnostic stemB and proB were identified and stable during
689 serial transplantation with identification of some mosaicism suggesting sub-clones in each
690 compartment. Relationships of transplants are indicated. Relapse stemB and proB were
691 genetically identical but stemB showed 90% mosaicism of all clones suggesting the
692 existence of a pre-leukemic clone. Deletions are shown in red and amplifications in blue.
693
694 **Figure 7: Pre-leukemic and leukemic hierarchy (Patient 4).** Based on genetic mosaicism
695 and different sizes of chromosome 7 and 14 deletions a pre-leukemic clonal hierarchy could

696 be constructed which showed clonal evolution at the pre-leukemic that gave rise to the
697 diagnostic leukemic sub-clones as well as evolving in another pre-leukemic sub-clone
698 responsible for relapse. Based on secondary transplantation assays, relapse but not
699 diagnostic cells displayed phenotypic plasticity.

700

701 **Supplementary Figures Legends**

702 **Figure S1: Flow cytometry sorting strategy.** Representative gating strategy used for the
703 analysis of immunophenotypically-distinct Down's syndrome ALL subpopulations before and
704 after xenotransplantation. StemB ($CD34^{+}CD38^{-/low}CD19^{+}$) and proB ($CD34^{+}CD38^{+}CD19^{+}$)
705 cells were sorted. **A-B**. Patient 2 and 3 leukaemia respectively.

706 **Figure S2: Cell cycle analysis. A.** Cell cycle analysis of representative xenografted stemB
707 and proB as compared to the **B.** patient relapse.

708 **Figure S3: RNA sequencing analysis. A-C** Gene Set Variation Analysis (GSVA) analysis
709 of RNA sequencing data looking at the expression of cell cycle related gene signatures. Six
710 different populations of cells were analysed: i) diagnostic stemB cells, ii) diagnostic proB
711 cells iii) relapse stemB cells harvested from secondary xenografts injected with stemB cells
712 isolated from primary xenografts iv) relapse proB cells harvested from secondary xenografts
713 injected with stemB cells isolated from primary xenografts, v) relapse proB cells harvested
714 from secondary xenografts injected with proB cells isolated from primary xenografts, and vi)
715 relapse stemB cells harvested from secondary xenografts injected with proB cells isolated
716 from primary xenografts. Within each heatmap samples are sorted by category and genes
717 split into top 500 most variable vs all others. **A.** G1/S gene signature[25], **B.** G2/M gene
718 signature[25], **C.** E2F targets gene signature[24] **C.** Gene set enrichment analysis (GSEA) for a
719 selection of MSigDB-50 Hallmark gene-sets[24] and published signatures associated with
720 predefined differentiation stages of the B-cell ontogeny[21]. This analysis looks specifically at
721 the top 500 genes driving clustering along the PC2 component of the PCA analysis. **D.** PCA
722 analysis based on bulk RNA sequencing of diagnostic and relapse cells harvested from
723 primary and secondary xenografts. Arrows showing the contribution of gene expression
724 signatures involved in BCR signalling and B-cell differentiation[22] are shown. Significance
725 thresholds: <0.05 after adjusting for multiple testing (using the Benjamini-Hochberg method).

Figure 1

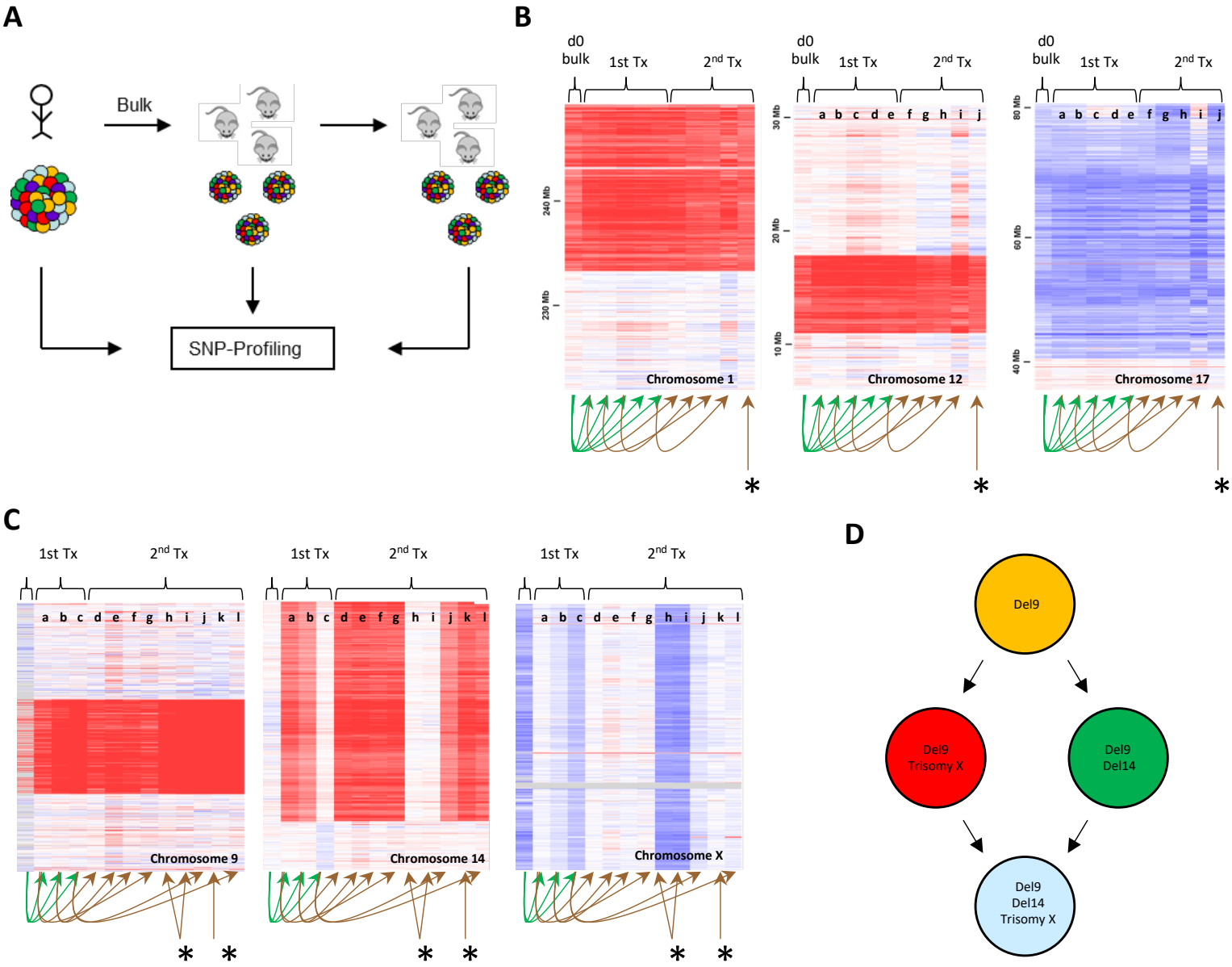
A
Bulk
SNP-Profiling
B
d0 bulk
1st Tx
2nd Tx
240 Mb
230 Mb
Chromosome 1
30 Mb
20 Mb
10 Mb
Chromosome 12
80 Mb
60 Mb
40 Mb
Chromosome 17
a b c d e f g h i j
C
a b c d e f g h i j k l
Chromosome 9
Chromosome 14
Chromosome X
D
Del9
Del9 Trisomy X
Del9 Del14
Del9 Del14 Trisomy X

Figure 2

A

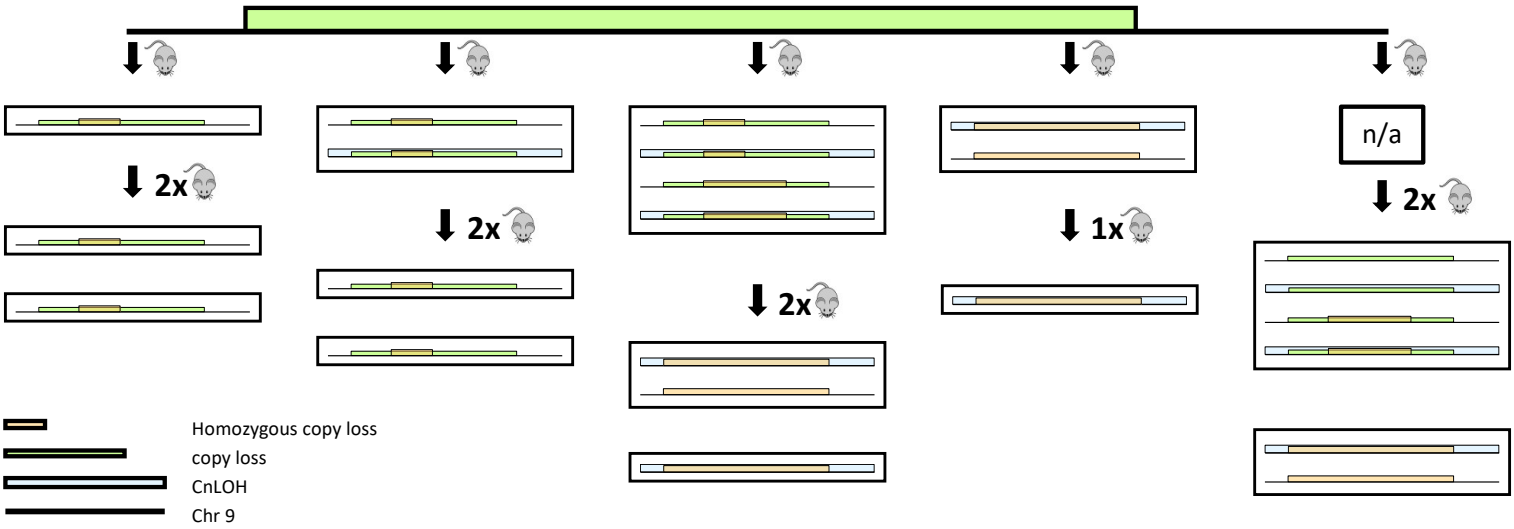
2x
2x
2x
1x
n/a
2x
Homozygous copy loss
copy loss
CnLOH
Chr 9

B

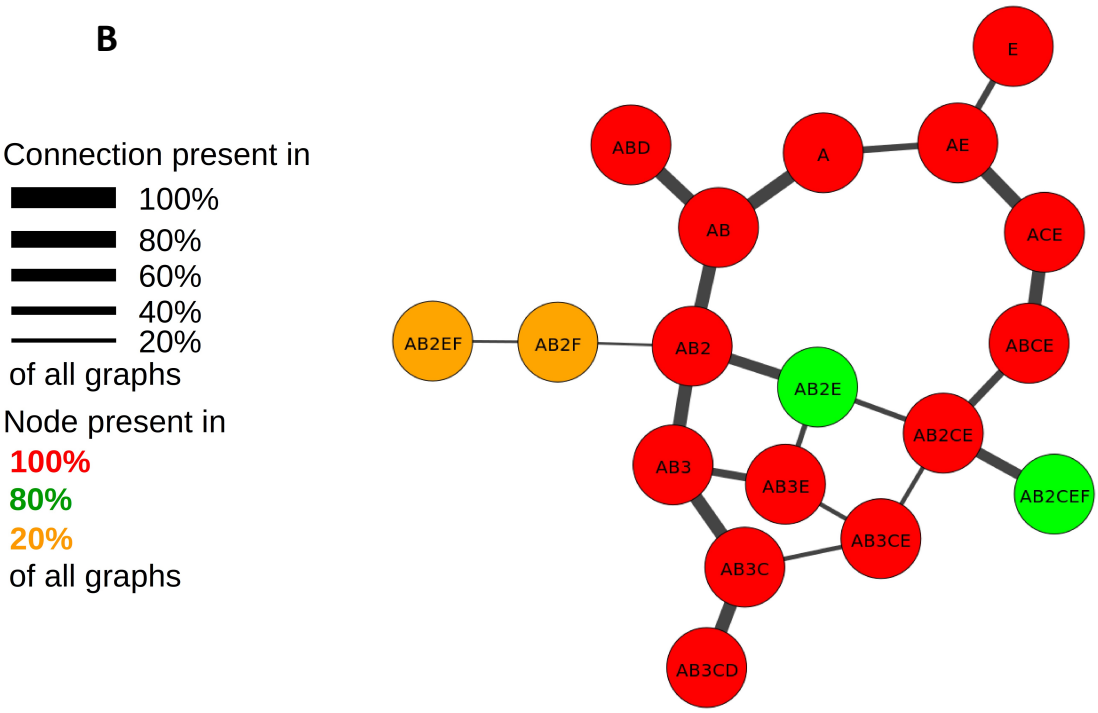
Connection present in
100%
80%
60%
40%
20%
of all graphs
Node present in
100%
80%
20%
of all graphs
E
ABD
A
AE
AB
ACE
AB2EF
AB2F
AB2
ABCE
AB2E
AB2CE
AB3
AB3E
AB2CEF
AB3CE
AB3C
AB3CD

Figure 3

A

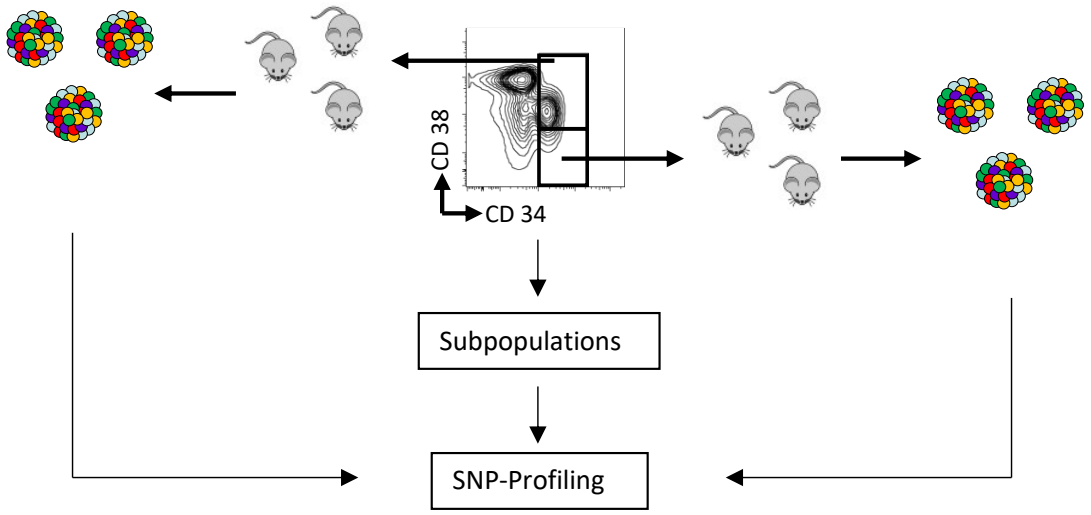
CD 38
CD 34
Subpopulations
SNP-Profiling

B

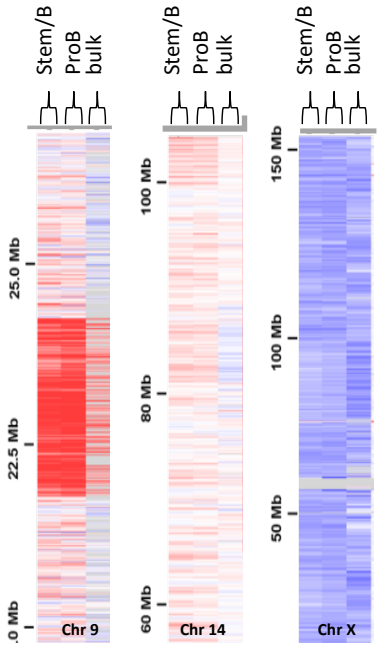
Stem/B
ProB
bulk
25.0 Mb
22.5 Mb
Chr 9
100 Mb
80 Mb
60 Mb
Chr 14
150 Mb
100 Mb
50 Mb
Chr X

C

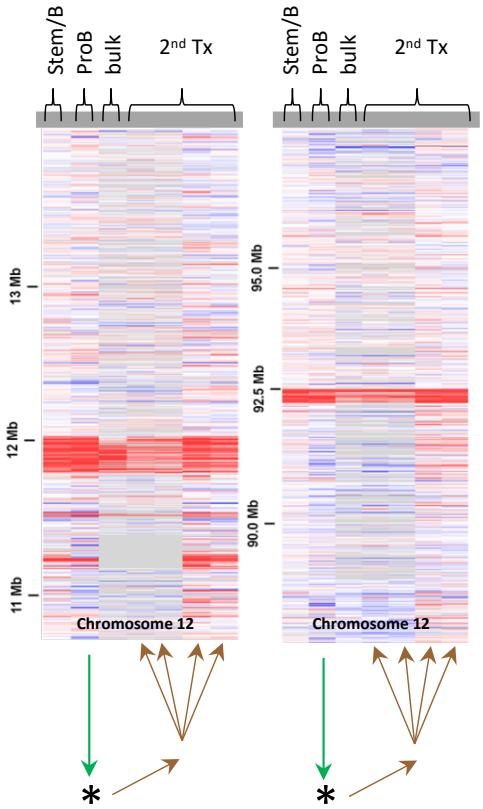
Stem/B
ProB
bulk
2nd Tx
13 Mb
12 Mb
11 Mb
Chromosome 12
95.0 Mb
92.5 Mb
90.0 Mb
Chromosome 12
*
*

Figure 4

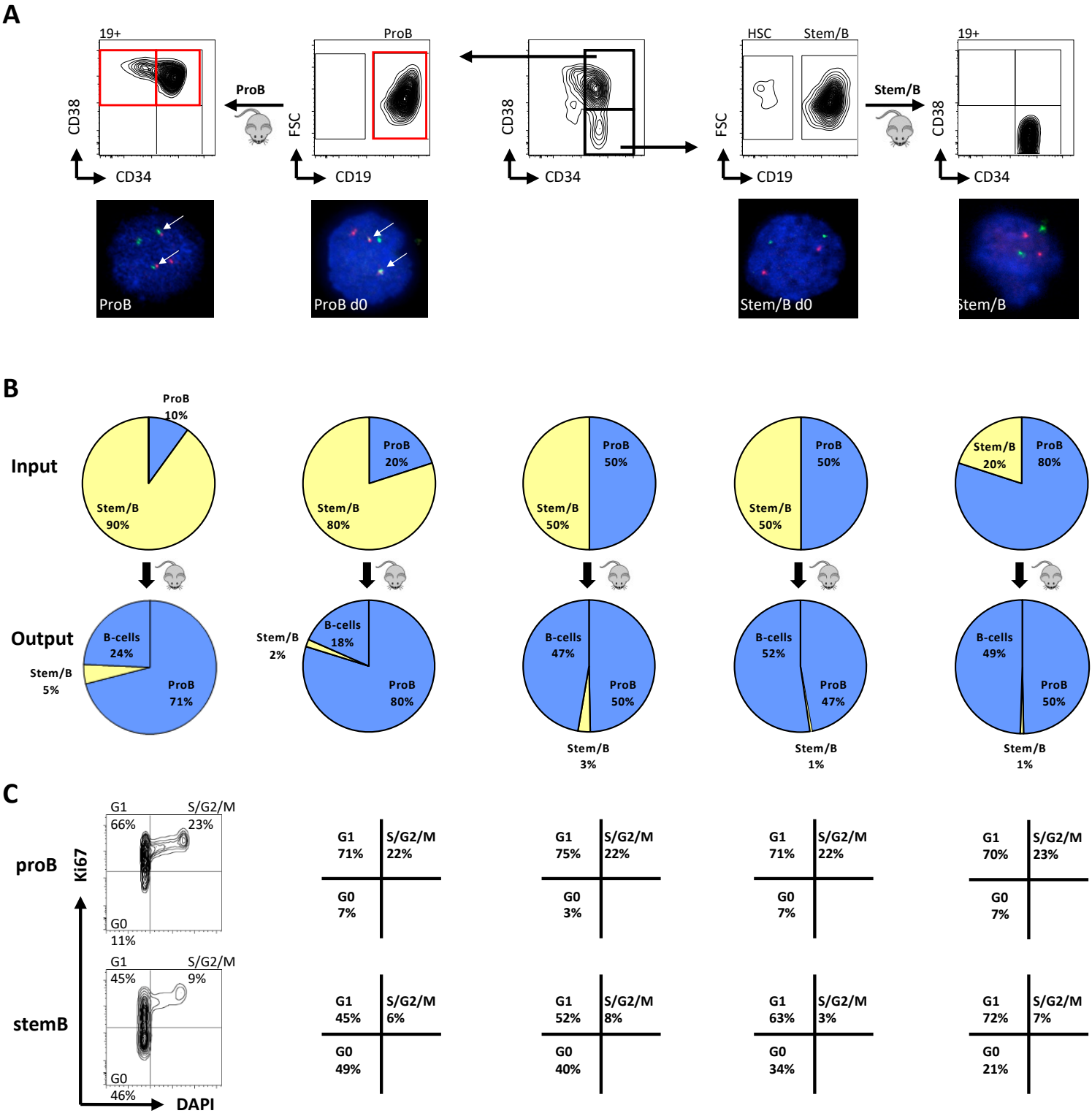
A
19+
CD38
CD34
ProB
ProB
FSC
CD19
CD38
CD34
HSC
Stem/B
FSC
CD19
Stem/B
19+
CD38
CD34
ProB
ProB d0
Stem/B d0
Stem/B
B
Input
ProB 10%
Stem/B 90%
ProB 20%
Stem/B 80%
ProB 50%
Stem/B 50%
ProB 50%
Stem/B 50%
Stem/B 20%
ProB 80%
Output
B-cells 24%
Stem/B 5%
ProB 71%
Stem/B 2%
B-cells 18%
ProB 80%
B-cells 47%
ProB 50%
Stem/B 3%
B-cells 52%
ProB 47%
Stem/B 1%
B-cells 49%
ProB 50%
Stem/B 1%
C
proB
stemB
Ki67
DAPI
G1 66%
S/G2/M 23%
G0 11%
G1 45%
S/G2/M 9%
G0 46%
G1 71%
S/G2/M 22%
G0 7%
G1 75%
S/G2/M 22%
G0 3%
G1 71%
S/G2/M 22%
G0 7%
G1 70%
S/G2/M 23%
G0 7%
G1 45%
S/G2/M 6%
G0 49%
G1 52%
S/G2/M 8%
G0 40%
G1 63%
S/G2/M 3%
G0 34%
G1 72%
S/G2/M 7%
G0 21%

Figure 5

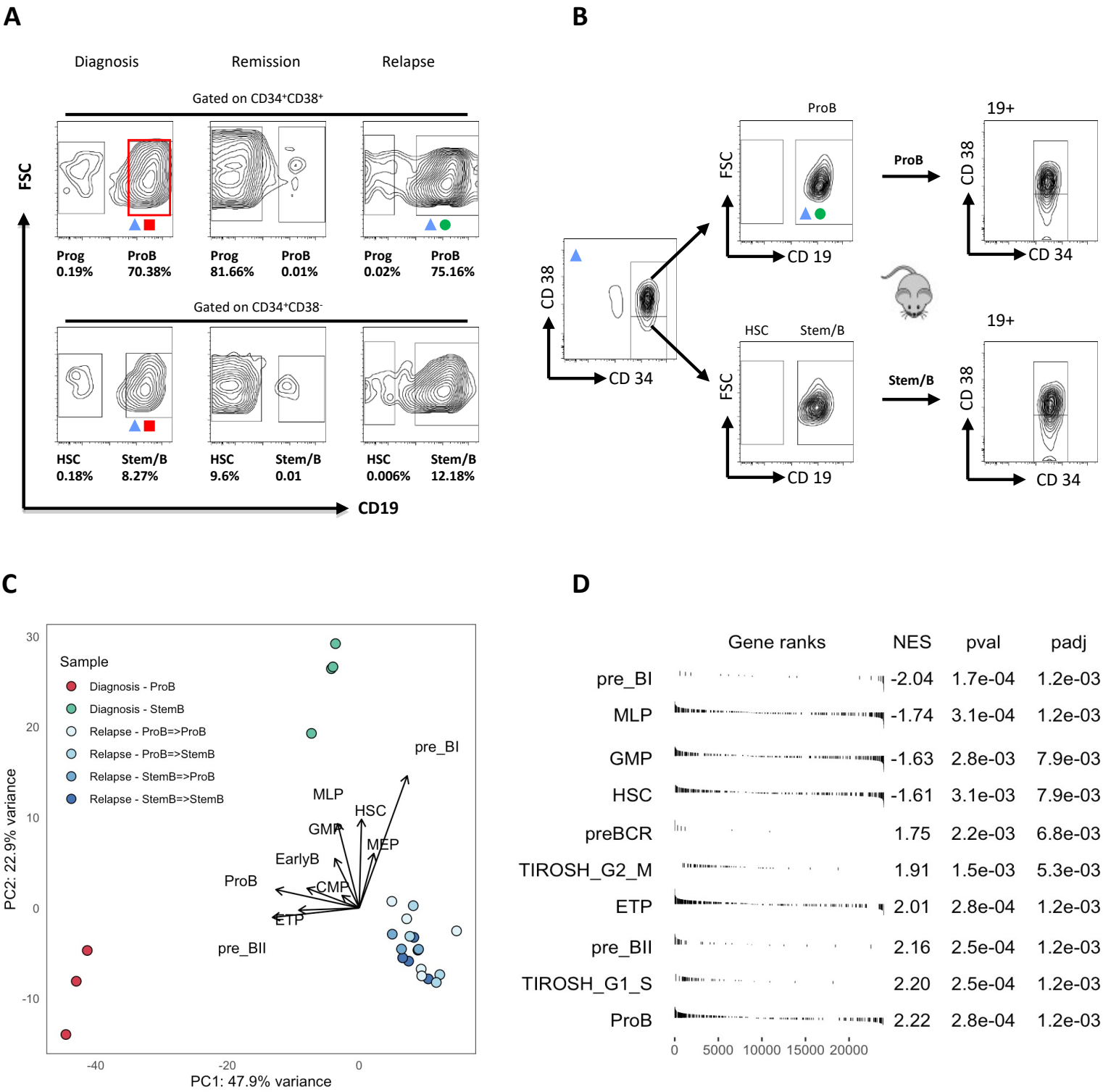
A
Diagnosis
Remission
Relapse
Gated on CD34+CD38+
FSC
Prog 0.19%
ProB 70.38%
Prog 81.66%
ProB 0.01%
Prog 0.02%
ProB 75.16%
Gated on CD34+CD38-
HSC 0.18%
Stem/B 8.27%
HSC 9.6%
Stem/B 0.01
HSC 0.006%
Stem/B 12.18%
CD19
B
ProB
19+
FSC
CD 19
CD 38
CD 34
HSC
Stem/B
C
Sample
Diagnosis - ProB
Diagnosis - StemB
Relapse - ProB=>ProB
Relapse - ProB=>StemB
Relapse - StemB=>ProB
Relapse - StemB=>StemB
pre_BI
MLP
HSC
GMP
MEP
EarlyB
ProB
CMP
ETP
pre_BII
PC2: 22.9% variance
PC1: 47.9% variance
D
Gene ranks
NES
pval
padj
pre_BI -2.04 1.7e-04 1.2e-03
MLP -1.74 3.1e-04 1.2e-03
GMP -1.63 2.8e-03 7.9e-03
HSC -1.61 3.1e-03 7.9e-03
preBCR 1.75 2.2e-03 6.8e-03
TIROSH_G2_M 1.91 1.5e-03 5.3e-03
ETP 2.01 2.8e-04 1.2e-03
pre_BII 2.16 2.5e-04 1.2e-03
TIROSH_G1_S 2.20 2.5e-04 1.2e-03
ProB 2.22 2.8e-04 1.2e-03
0 5000 10000 15000 20000

Figure 6

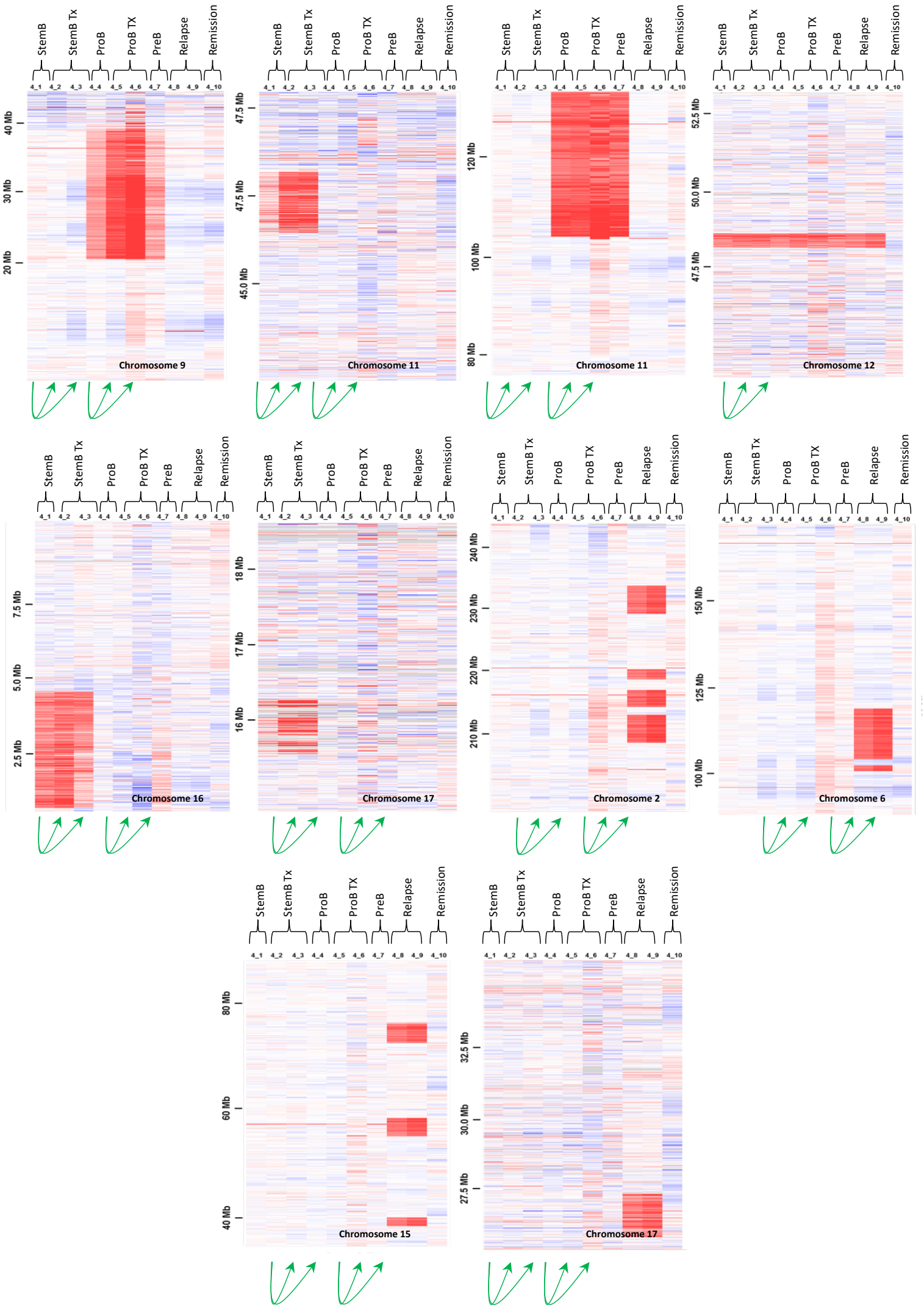
StemB
StemB Tx
ProB
ProB TX
PreB
Relapse
Remission
4_1 4_2 4_3 4_4 4_5 4_6 4_7 4_8 4_9 4_10
40 Mb
30 Mb
20 Mb
Chromosome 9
47.5 Mb
47.5 Mb
45.0 Mb
Chromosome 11
120 Mb
100 Mb
80 Mb
Chromosome 11
52.5 Mb
50.0 Mb
47.5 Mb
Chromosome 12
7.5 Mb
5.0 Mb
2.5 Mb
Chromosome 16
18 Mb
17 Mb
16 Mb
Chromosome 17
240 Mb
230 Mb
220 Mb
210 Mb
Chromosome 2
150 Mb
125 Mb
100 Mb
Chromosome 6
80 Mb
60 Mb
40 Mb
Chromosome 15
32.5 Mb
30.0 Mb
27.5 Mb
Chromosome 17

Figure 7

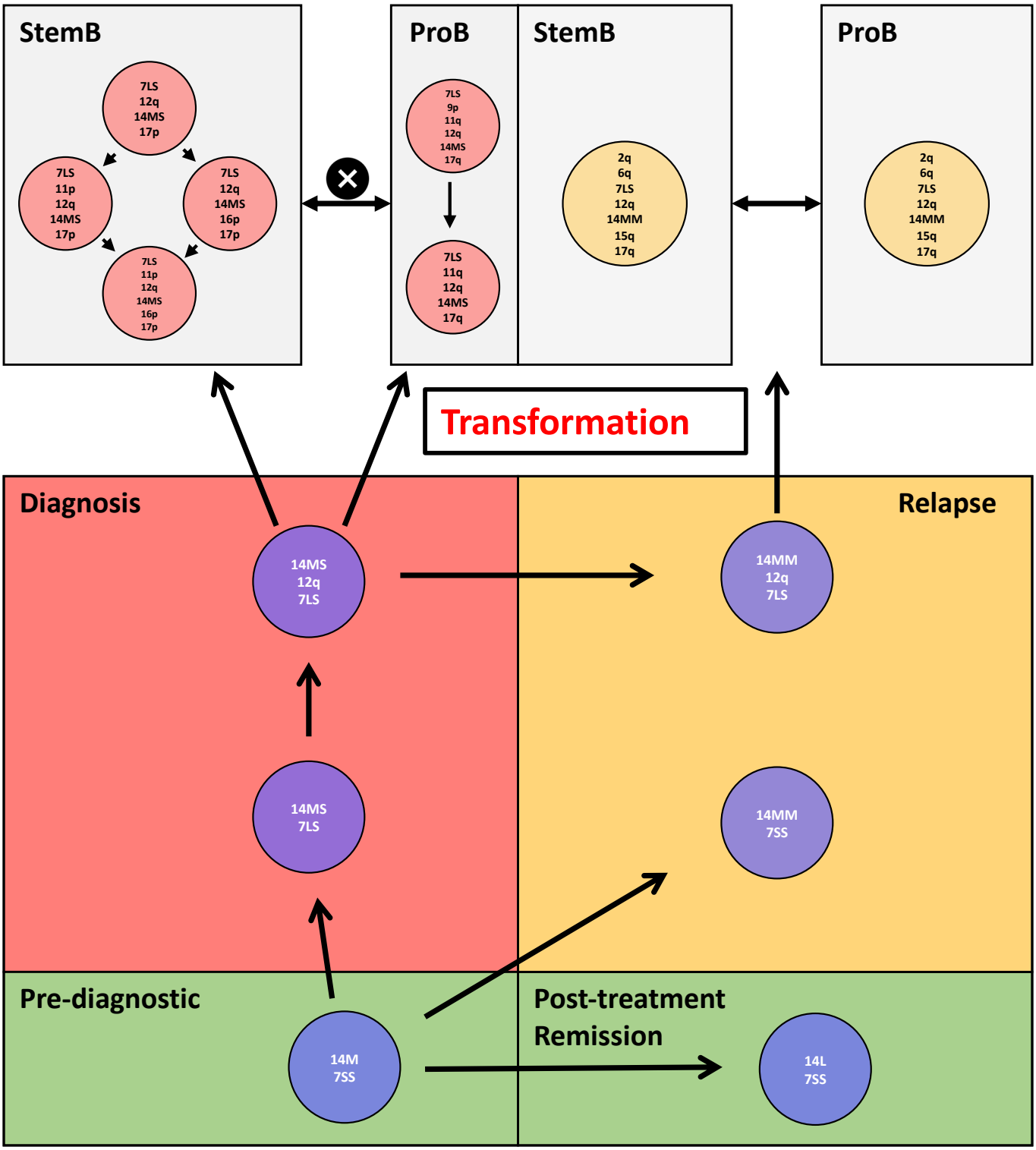
StemB
7LS
12q
14MS
17p
7LS
11p
12q
14MS
17p
7LS
12q
14MS
16p
17p
7LS
11p
12q
14MS
16p
17p
ProB
7LS
9p
11q
12q
14MS
17q
7LS
11q
12q
14MS
17q
StemB
2q
6q
7LS
12q
14MM
15q
17q
ProB
2q
6q
7LS
12q
14MM
15q
17q
Transformation
Diagnosis
14MS
12q
7LS
14MS
7LS
Relapse
14MM
12q
7LS
14MM
7SS
Pre-diagnostic
14M
7SS
Post-treatment
Remission
14L
7SS